ON RELATION OF MESO-α INERTIA WAVE DEVELOPMENT TO RAINSTORM ENHANCEMENT IN TYPHOON POLLY

Ding Zhiying (丁治英) and Chen Jiukang (陈久康)

Nanjing Institute of Meteorology, Nanjing, 210044

Received 3 May 1995, accepted 6 December 1995

ABSTRACT

Numerical simulation and diagnosis show that the amplified rainstorm from Typhoon Polly is related to the development/migration of meso-α gravity waves, inhomogeneous stratification distribution and cumulus convection latent heating feedback in the storm; such waves at a large scale are excited by large-scale nonlinear advection; substantially amplified ageostrophic wind perturbation resulting from the latent heating gives rise to intensified wave amplitude, leading to enhanced rising and thus torrential rainfall; as the waves migrate towards reduced stability, wave energy is most likely to increase.

Key words: typhoon, cumulus convection, gravity-inertia wave (GIW), rainstorm

I. INTRODUCTION

Gravity-inertia waves (GIWs) in typhoon have long been recognized in a meteorological context but it is difficult to make analysis of it in operational practice because of its short wave length, small domain and rapid change. As such, study of the development and relation to torrential rain from a typhoon by way of numerical modeling is worthwhile. For this purpose, numerical experiment was conducted with the typhoon in the period 20 h August 31 through 20 h September 1, 1992 and its associated rainfall enhancement, alongside with diagnosis of the simulations. Detailed investigation was executed of meso-α GIWs emerging in a typhoon, relevant ageostrophic wind and inhomogeneous stratificatin in an attempt to uncover the relationship between such waves and rainfall.

II. WEATHER PATTERN AND MODEL USED

Landing at 0800 LST, August 31, 1992 in the vicinity of Fuzhou, Typhoon Polly spread rainstorm along its path, especially when passing through eastern Shandong and Liaoning. It moved out of northern Jiangsu to the sea at 2000 LST, September 1, with somewhat reduced vigor and as depicted in surface to 500-hPa charts, Polly's center was inclined westward in a baroclinic state without much shrink in size. It had pronounced influence on eastern China.

Analysis based on cloud maps and numerical results (Ding and Chen, 1997) show that the rainstorm enhancement was related largely to strengthened cumulus convection to the south, which intensified low-level jet streak and northward transport of momentum and energy, thereby causing rainfall enhancement, whose relation to the development of GIWs is dealt with in this study.

The model used is the MM4 form of Anthes (1987). It has grid spacing of 90 km (total grid points of 46×46) with the computational center at 36°N, 117°E. For the typhoon four experiments were conducted: Exp. 1 is the control one, Exp. 2 the one of no cumulus convection latent heating, Exp. 3 of no large-scale condensation heating, and Exp. 4 of no heating of both origins.

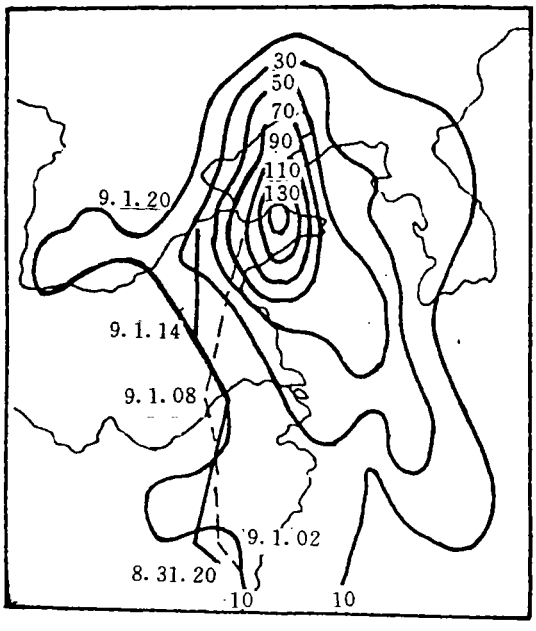

Fig. 1. Path of Polly and 24-h forecast rainfall, with the observed (predicted) path indicated by solid (dotted) line.

Results from the control experiment were in rough agreement with the observed (Fig. 1), showing the maximum rainfall of 188 mm in the neighborhood of Dalian compared to 211 mm measured at the city with typhoon's path close to the observed. For details the reader is referred to Ding and Chen (1997).

Ⅲ. AGEOSTROPHIC WIND FIELD OF THE TYPHOON

GIWs developing in a typhoon depend on ageostrophic wind activity and evolution. Therefore, calculation done of model output at a 6-h interval from Exps. 1-4 to investigate the relation of ageostrophic wind to these waves and torrential rain. Analysis of ageostrophic wind of the model extent discovers two maxima, one at 1000-700 hPa and the other around 200 hPa, with focus on ageostrophic fields at 850 and 200 hPa levels for detailed study.

Based on the first 6-h integration from Exp. 1 a more vigorous supergeostrophic wind band emerges in the vicinity of the hyetal region (maximum $u - u_g$ of 27 ms^{-1}) which is inside an ageostrophic convergence zone, with maximum precipitation of 45 mm/6h, compared to the 200-hPa counterpart in an ageostrophic divergence zone. 12-h integration shows that 850-hPa ageostrophic wind gets considerably strengthened with $u - u_g$ increased to 48 ms^{-1} (Fig. 2) and $v - v_g$ to 44 ms^{-1}, and the hyetal belt remaining in the ageostrophic convergence zone, whose central maximum rainfall is 78/6h, compared to 200-hPa supergeostrophic wind of 29 ms^{-1}. Observation made at the coastwise station of Chenshantou, Shandong, shows the 850-hPa wind of 50 ms^{-1} at 0800 LST, September 1 of the year. So, quite probable is the ageostrophic wind of such velocity.

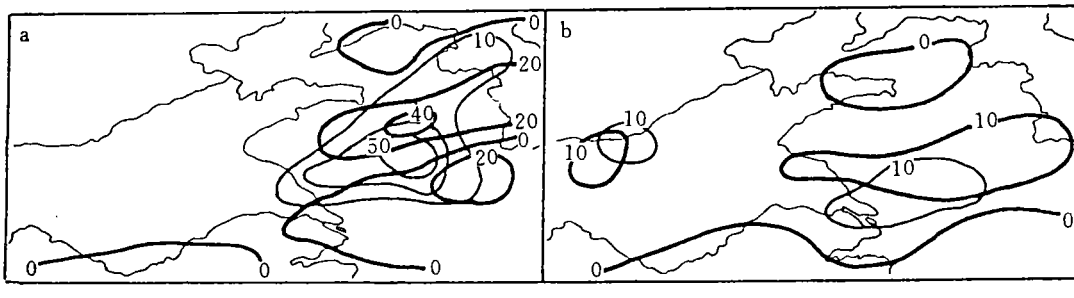

Fig. 2. 850 hPa $u-u_g$ pattern collocated with a 3-h hyetal band after 12-hr integration from Exp. 1(a) and Exp. 2(b).

The 18-h integration shows that 850-hPa $u-u_g$ is slightly reduced in its central value but intensified in the situation as a whole with its size expanded. Maximum $u-u_g$ is 42 and $v-v_g$ grows to 54 $ms^{-1}$for its center with the rainfall center remaining in the field of low-convergence and high-level divergence as presented in the diagram at hour 12 integration. The central value of 200 hPa $v-v_g$ is increased to 46 ms^{-1}, causing the rain-band to enlarge and move northwestward at greater velocity but with the central 6-h precipitation of 56 mm, a quantity somewhat less than that (78 mm) at hour 12 integration.

The 12-h integration indicates that maximum 850-hPa $u-u_g$ increases considerably, reaching 63 ms^{-1}as compared to that obtained 6 hours previously, with the central rainfall of 99 mm/6 h whilst the $v-v_g$ field is basically maintained and the high-level situation kept unchanged in comparison to the previous pattern.

It is evident from Fig. 2a that the weak ageostrophic wind is observed in the vicinity of the typhoon's center with the strongest adjacent to the hyetal region that is marked by ageostrophic convergence (divergence) at low (high) levels, such being the case on all the 6-h integrations. From the foregoing analysis one can also see that the torrential rain event bears a close relation to the amplified supergeostrophic wind. As evidenced from Fig. 2, however, the subgeostrophic wind gets greatly intensified concurrently with the enhanced supergeostrophic wind, with the central rain-band generally located around the zero line between the super-and subgeostrophic winds, the latter being weaker.

Exp. 2 is the one with cumulus convection latent heat release removed, resulting in a greatly decayed ageostrophic wind. Based on the first 6-h integration, 850-hPa $u-u_g$ has its central value of 21 and $v-v_g$ of 14 ms^{-1}, with the central rainfall of 21 mm only and the hyetal area around the field of low-and high-level ageostrophic convergence and divergence, respectively. The 12-h integration shows further weakening of the ageostrophic wind, leading to the central $u-u_g$ of 17 and $v-v_g$ of 14 ms^{-1} (see Fig. 2b) and the central rainfall of 22 mm/6h. The 18-h integration indicates that the ageostrophic component keeps reducing, leading to $u-u_g$ of 13 ms^{-1}in contrast to the 24-h results which shows that the central $u-u_g$ has value of 17 $ms^{-1}$and $v-v_g$ of 22 $ms^{-1}$with the central precipitation increased to 30 mm/6h. It follows that the large-scale latent heating exerts intensified impact on the ageostrophic wind in this interval of integration.

Exp. 3 is the one with large scale condensation latent heating removed, showing the ageostrophic wind changing in much the same way as in Exp. 1. It should be noted that $u-u_g$ increases by 21 ms^{-1} over the 6-h integration (from hr. 18～24) in Exp. 1 is in contrast to the decrease of 3 ms^{-1}in Exp. 3 with slightly changed $v-v_g$, which is likely to relate to the interaction between system of different scales. From Exp. 2, clearly, the 24-h integrated large-scale latent heat has its contribution enhanced to the ageostrophic wind and presumably plays a role in strengthening cumulus convection. The θ_{se} analysis shows that the 4th interval (hr. 18～24) represents the period for the southward migration of the northern frontal zone to be connected with the studied typhoon and the frontal effect may be the cause of enhancing the large-scale latent heat impact.

Exp. 4 yields the results basically identical to those of Exp. 2, with the difference in the ageostrophic wind ranging over 1～2 ms^{-1}. It is evident that the ageostrophic wind enhancement is mainly associated with latent heat release from cumulus convection whilst large scale latent heat and nonlinear advection exert no significant effect. Inspection of the ageostrophic center changing as a function of altitude based on 12-h integra-

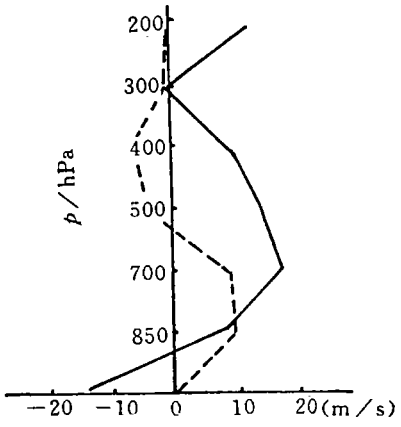

Fig. 3. $u-u_g$ (ms^{-1}) field through the rainstorm center in the whole extent, based on 12-h integration, with Exp. 1 denoted by full and Exp. 2 by dotted line.

tion (Fig. 3) shows that the wind is faint around the rainfall center and $\frac{\partial u - u_g}{\partial z} > 0$, $\frac{\partial u - u_g}{\partial z} < 0$, $\frac{\partial u - u_g}{\partial z} > 0$ below 700 hPa, around 700~300 hPa and 300~200 hPa, respectively. Results from Exps. 1 and 2 are in rough agreement with each other. Their comparison shows that $u - u_g$ in the precipitating center of Exp. 2 is much smaller than that of Exp. 1 and the higher the level is, the closer it is to zero. Besides, the 200-hPa ageostrophic intensification is related to cumulus convection over the rainstorm band.

From the foregoing analysis one can see that cumulus has an enormous influence on the enhancement of the ageostrophic wind, which, in turn, bears an intimate relation to the rainstorm's vigor. It follows from the relation between ageostrophic wind and GIWs that cumulus convection serves as the major factor for the genesis/development of such waves.

Ⅳ. GRAVITY-INERTIA WAVES IN TYPHOON POLLY

Li (1978) indicated that GIWS made appearance in a low-level physical-quantity field as a $\pi/2$ difference between vorticity and divergence with the convergence center matching the region of vertical rising, propagating as waves. The field featured by such waves were discovered in the present simulations.

Fig. 4a is a plot of 850-hPa vorticity/divergence distribution from 12-h integration. Such a situation presents itself to the northeast of Polly. The zero line of divergence passes through the maximum vorticity center and the centers of divergence, convergence, vertical rising and precipitation are distributed in such a manner as to exhibit rather typical gravity-inertia waves (figure not shown), which being on a larger scale, differ from those in the form of a spiral rain-band in a typhoon, falling into a category of meso-α GIW feature.

By definition of GIWs, vertical speed represents another form of their amplitude, identical in magnitude to wave energy. Inspection of Table 1 shows that the integration in the first 18 hours gives a period of energy growth, which is kept almost unchanked subsequently. Such a situation came somewhat later as compared to the measured cloud development in the interval 1200 GMT, August 31 to 0000 GMT, September 1, 1992 in the eastern seaboard, including Shandong Peninsula. Nevertheless, the simulated general trend is close to the observed.

Table 1. Vertical rising ($10^{-4}hPa^{-1}$) simulated from Exps. 1 and 2.

Hour of integration	06	12	18	24
Exp. 1	−159	−174	−204	−201
Exp. 2	−50	−39	−61	−82

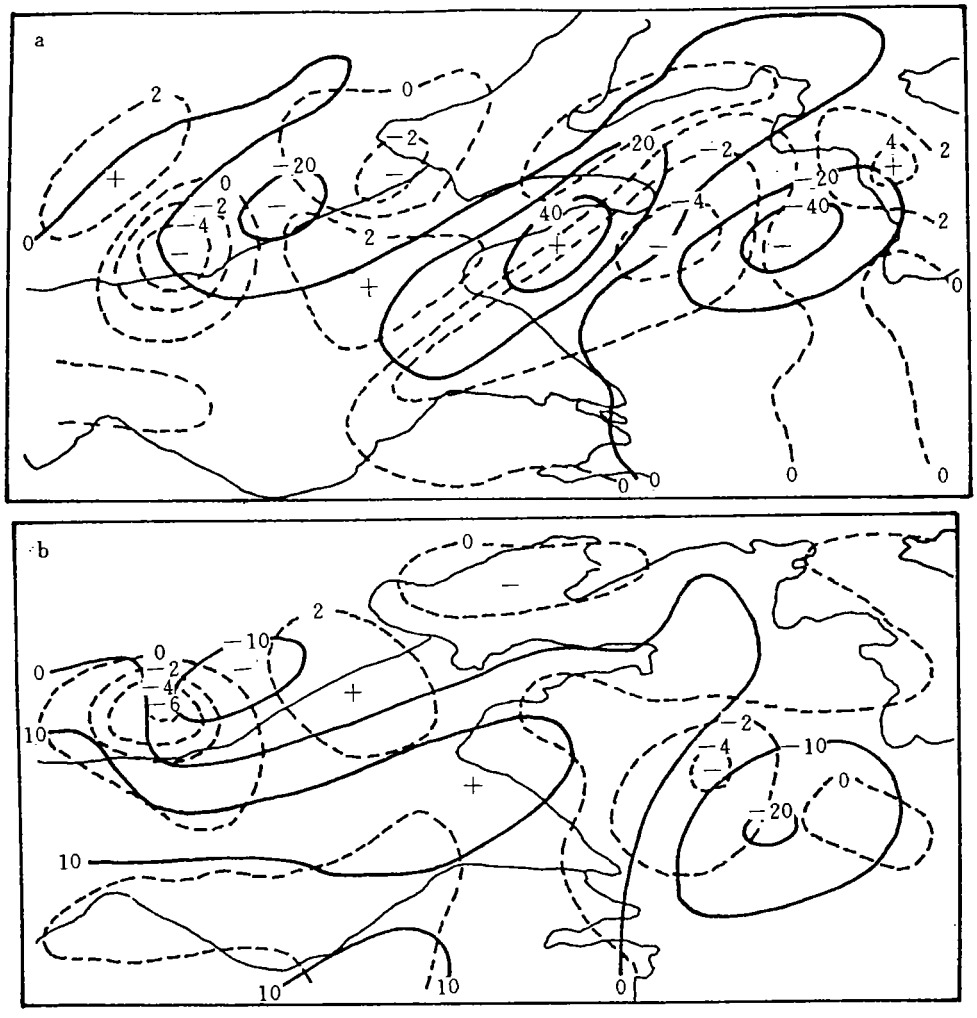

Fig. 4. 850 hPa vorticity ($10^{-5}s^{-1}$, solid line) and divergence ($10^{-6}s^{-1}$, dotted) prepared from 12-h integration, with Exp. 1 in (a) and Exp. 2 in (b).

Based on integration from hr. 12～18, the center of wave energy migrates northwestward, yielding downstream effects, causing the development of GIWs in eastern Shandong and thus the enhanced torrential rain in that area.

Energy in such waves was induced substantially in the absence of cumulus convection latent heating (Exp. 2) and central vertical rising dropped, on average, by 12.6×10^{-3}hPa s^{-1}. Inspection of Table 1 shows gradual growth in the wave energy in this experiment with the propagation almost identical to that revealed in Exp. 1.

Fig. 4b shows the simulation from Experiment of no cumulus convection latent heating, indicating that the GIWs remain visible only with weakened vigor and elongated wavelength. It is apparent that the meso-*a* GIWs in the studied typhoon were generated not by in-typhoon cumulus convection but by the ageostrophic field in the large-scale environmental field. Also, the wave pattern is not so clear as that from Exp. 1, which was perhaps associatd with enfeebled ageostrophic perturbation, leading to reduced GIWs, and reinforced effect of waves of other types when cumulus convection feedback was removed.

Analysis indicates that cumulus convection is the leading factor of intratyphoon GIWs development but not the exclusive cause of their genesis. Such waves gave rise to enhanced rainstorm over the Shangdong Peninsula and its vicinity through downstream effect. These waves were produced by the ageostrophic field and intensified with amplified amplitude due to cumulus convection condensation feedback so that the amplitude and rising were strengthened, which, in turn, led to amplified ageostrophic perturbation. Such feedback promoted most favourably the rainstorm enhancement.

The wave variation from Exps. 3 and 4 are basically similar to that from Exp. 1, illustrating weak influence on the studied waves of large-scale condensation latent heating. Also, we can see that these waves are generated mainly by large-scale nonlinear advection and enhanced under the effect of cumulus convection, leading to the amplified torrential rain.

V. INHOMOGENEOUS STRATIFICATION AND GIW DEVELOPMENT

Upon simplifying the equation of motion and using the WKBJ technique, Zhao and Shun (1990) proposed the equation of gravity-inertia wave energy of the form

$$\frac{\partial}{\partial T}\iint_s E\mathrm{d}s = -\iint_s \frac{K_h}{2\omega^2 K^2} E \frac{\partial N^2}{\partial T}\mathrm{d}s - \iint_s \frac{E}{N^2 - f^2}\vec{C}_g \cdot \nabla N^2 \mathrm{d}s$$

where E represents the wave energy, $K^2 = K_h^2 + \tilde{n}^2$, in which $K_h(\tilde{n})$ is the wave number horizontally (vertically), N^2 the Brunt-Väisälä frequency, f the Coliolis parameter, $\vec{C}_g$ the wave-ensemble velocity and ω the angular speed. The first term on the r.h.s stands for the effect of change in stability on wave energy, which increases as the stability decreases with time. The second term means that for stratification, both steady and unsteady, the energy increases as the waves move towards reduced stability or enhanced instability, and vice versa. It is, therefore, necessary to examine the contributions of N^2 (stability) and ∇N^2 (inhomogeneous stratification) to the development of meso-α GIWs in a typhoon.

Comparison of N^2 field from Exp. 1 to those from Exps. 2 and 3 shows that all the N^2 patterns are highly similar to each other, thereby indicating very weak influence on atmospheric stratification distribution of cumulus convection an large-scale condensation latent heating. The central value of Exp. 2 instability was little higher as compared to that of Exp. 1, a result that may be related to the fact that unsteady energy was unable to be completely released after cumulus convection was removed. And the central value was the same from Exp. 3 as from Exp. 1.

It was found in Exp. 1 that for wave energy increasing domain the 0-12 h integration resulted in $\partial N^2/\partial T < 0$, favouring the energy growth; the 12-24 h run led to $\partial N^2/\partial T \sim 0$, unfavourable for the growth, a result that agrees with that of the 18—24 h integrating interval for slowly developing GIWs (cf. Table 1). On the other hand, the 12-18 h integration in the same experiment showed that the waves were developing at greater intensity. The reason is thought to be associated with the distribution of uneven stratification.

Also, in the analysis of $\partial N^2/\partial X$, $\partial N^2/\partial Y$ fields, it is found that wave energy increases as the waves migrate towards reduced stability. By the GIWs definition, the energy increases (decreases) agree with the growth (reduction) of vertical velocity and the energy

propagates in the direction perpendicular to the group velocity: $\vec{C}_g \cdot \vec{C} = 0$, so that the direction of GIWs traveling can be inferred if such waves are developing as the simulation predicts. Prior to hour 12, wave energy migrated dominantly northward and $\partial N^2/\partial X < 0$ in the direction in which the GIWs traveled, a situation that favoured their development and agree with the simulated wave evolution. Fig. 5a illustrates the 850-hPa $\partial N^2/\partial Y$ pattern over 12-h integration in Exp. 1. Wave energy obtained from the 12-18 h run indicates the wave energy propagation from east to northwest; $\partial N^2/\partial Y < 0$ in the x-direction means little contribution to the GIW; $\partial N^2/\partial Y < 0$ in the y-direction the GIW traveled. It follows that, on the whole, the uneven stratification pattern favoured the development of such waves. Vertical motion strengthened upon 18-h integration and such was basically the case for the 18-24 h run and wave energy got basically maintained under the effect of the two factors.

Based on 12- h integration with no cumulus convection considered (Exp. 2), the inhomogeneous stratification pattern was much the same as that from Exp. 1 whereas the pattern from the run at hours 18～24 experienced little change. It follows that the uneven stratification pattern did not matter much to cumulus convection latent heating.

The 12-h integration (Fig. 5b) exhibits two centers of vertical speed. The western one has its wave energy propagating in the west so that the GIW should move northward; the wave energy is centered in the region of $\partial N^2/\partial Y > 0$ from the $\partial N^2/\partial Y$ pattern; the central vertical speed reduces from -83×10^{-4}hPa s^{-1} (12-h integration) to $-61\times$

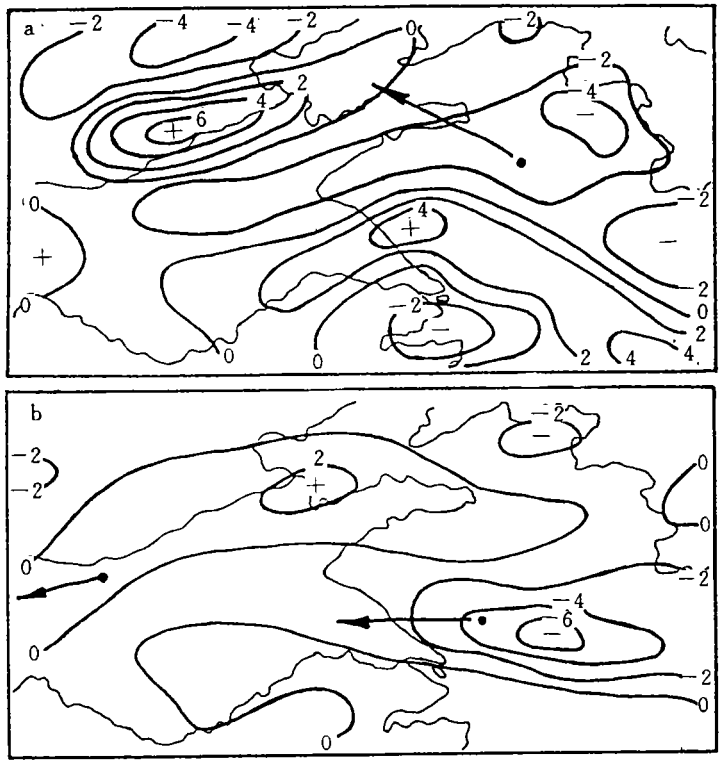

Fig. 5. Change in $\partial N^2/\partial Y$ ($10^{-9}\cdot m^{-2}\cdot s^{-1}$) and the center of vertical speed, based on 12-h integration. Arrow denotes the direction of ω center's movement based on 18-h run. a) Exp. 1, b) Exp. 2.

10^{-4}hPa s^{-1} (18-h run) with the center kept where $\partial N^2/\partial Y > 0$. And the eastern center keeps moving west and vertical speed grows with time (cf. Table 1) inside the region of $\partial N^2/\partial Y$, which is evidently associated with the fact that the GIW traveling towards reduced stability allows wave energy to grow in amount.

The uneven stratification pattern and change in wave energy from Exp. 3 is the same as from Exp. 1.

VI. CONCLUDING REMARKS

From the foregoing analysis, we reach the following.

a. In-typhoon meso-α GIW are generated under the action of nonlinear advection, depending predominantly on cumulus convection latent heating, ageostrophic wind and uneven stratification patterns for development, and slightly on large-scale condensation latent heating.

b. Cumulus convection and large-scale latent heating, feedback exert negligible impact on inhomogeneous stratification distribution and change in atmospheric stability.

c. Cumulus convection latent heating feedback is strongly responsible for enhanced ageostrophic wind and reinforced amplitude of GIW, which get greatly reduced in the absence of the feedback. With the feedback present, intensified GIWs lead to amplified rising motion that favours the enhanced rainstorm.

d. The strengthened amplitude of GIW influence was uneven stratification pattern. That is, however, much weaker as compared to the effect exerted by cumulus convection latent heating feedback. This can be made clear from the fact that with no such convection available, even though inhomogeneous stratification distribution promotes GIW development, no such waves are produced that are strong enough to cause amplified torrential rainfall.

REFERENCES

Anthes R A, Hsie E Y, Kuo Y H, 1987. Description of the Pnne State/NCAR mesoscale model version 4 (MM4), NCAR Tech. Note, NCAR/TN—282+STR, 66p.

Ding Zhiying, Chen Jiukang, 1997. Study on discontinuous northerly jump of an inland typhoon in relation to torrential rain. *J. Appl. Meteor.* **8** (1): 44-52 (in press, in Chinese with English abstract).

Li Maicun, 1978. Triggering of gravity waves to exceptional torrential rain, *Acta Atmospherica Sinica*, **2** (3): 201-210 (in Chinese with English abstract).

Zhao Ping, Sun Shuqing, 1990. On development of gravity-inertia waves in an inhomogeneously-stratified atmosphere, *Acta Meteorologica Sinica*, **48** (4): 397-403 (in Chinese with English abstract).